Phase separation in crystallizable multiblock poly(ether–ester) copolymers with poly(tetramethylene isophthalate) hard segments

R. A. Phillips* and S. L. Cooper†
Department of Chemical Engineering, University of Wisconsin-Madison, Madison, WI 53711, USA
(Received 28 December 1993)

The process of isothermal crystallization and phase separation in poly(tetramethylene isophthalate) (PTMI) and multiblock copolymers of PTMI with poly(tetramethylene oxide) (PTMO) is examined by differential scanning calorimetry. Morphology development is studied from the supercooled liquid to the completion of crystallization for compositions ranging from 30 to 100 wt% PTMI over a wide range of isothermal crystallization temperatures. A model is suggested whereby phase separation in the copolymers proceeds in a manner similar to crystallization of the homopolymer, implying phase-mixed non-crystalline regions with inhomogeneous mobilities. The experimentally observed multiple endotherm behaviour in the PTMI/PTMO copolymers is a characteristic of the hard segment, and is also observed in the PTMI homopolymer.

(Keywords: isothermal crystallization; phase separation; multiblock copolymers)

INTRODUCTION

Multiblock copolymers are an important group of thermoplastic elastomers. These materials rely on phase separation of the dissimilar blocks along the chain to impart their unique and useful mechanical properties in the solid state. Many important classes of these copolymers, such as polyurethane multiblock copolymers[1] and poly(ether–ester) multiblock copolymers[2], also contain sequences which are crystallizable. Relatively few studies have been performed which examine the dynamics of morphology development in semicrystalline multiblock copolymers.

Studies of morphology development in semicrystalline polyurethane multiblock copolymers have perhaps been most extensive[3–6]. These materials exhibit rich multiple endotherm behaviour depending on thermal history[5,7–12]. Although crystallinity is an important feature in these materials, the hard segments in polyurethanes can be strongly self-associating without crystallization[13]. Studies have attempted to investigate the phase separation/crystallization process in these materials through experiments addressing phase separation and phase dissolution[5,10–12], and the relationship to the observed thermal behaviour. Multiple endotherms are not unique to these systems, and are more generally observed in a wide variety of semicrystalline materials. It is of interest in this work to investigate which aspects of this general feature in semicrystalline polymers are observed in a multiblock copolymer where, in the absence of crystallinity, the self-association of the dissimilar segment types is not strong. Studies of phase separation in strongly crystallizable multiblock copolymers also provide an important limiting case for this general class of copolymer architecture.

Poly(ether–ester) copolymers have a multiblock chain architecture with alternating short chain polyester 'hard segments' and polyether 'soft segments'. The majority of studies for poly(ether–ester) copolymers have focused on materials with poly(tetramethylene terephthalate) (PTMT) hard segment sequences and poly(tetramethylene oxide) (PTMO) soft segment sequences. The morphology of these copolymers has been extensively characterized[14–26]. The general features of the morphology in these systems was detailed in early work by Cella[14] and remain to a large degree unchanged. The key features of this description include the crystalline polyester hard segments and an amorphous mixture (with comparatively low glass transition temperature, T_g) composed of polyether soft segments and 'dissolved' non-crystalline hard segments which are unable to crystallize. Multiple endotherms have been observed in PTMT/PTMO copolymers[25,26], and the PTMT homopolymer[26–28]. It is generally accepted that hard segment crystallization is a controlling factor governing the formation of physical crosslinks and subsequent mechanical properties. However, direct experimental observation of morphology development in the PTMT/PTMO copolymers is elusive owing to the high rate of crystallization of the PTMT sequences.

Crystallization of the hard segment sequences can be slowed by incorporation of the isomer poly(tetramethylene

*Current address: HIMONT USA Inc., Research & Development Center, Elkton, MD 21921, USA
†To whom correspondence should be addressed. Current address: College of Engineering, University of Delaware, Newark, DE 19716, USA

0032-3861/94/19/4146–10

isophthalate) (PTMI) in the hard segments[23,29–31]. Stevenson and Cooper[30] monitored the structural changes accompanying crystallization in moulded samples of PTMI/PTMO copolymers at room temperature using small angle X-ray scattering (SAXS) and differential scanning calorimetry (d.s.c.). The changes in mechanical properties accompanying crystallization in this system were attributed to a microstructural transformation associated with the development of the crystalline morphology. Recent work has demonstrated that PTMI/PTMO copolymers exhibit homogeneous melts which extend to temperatures below the hard segment melting point[31]. The present studies utilize these slowly crystallizing materials to examine the phase separation/crystallization process during morphology development in d.s.c. experiments which monitor the glass transition and multiple melting behaviour.

EXPERIMENTAL

The poly(ether–ester) copolymers were synthesized using standard procedures[32] from poly(tetramethylene ether) glycol ($M_n = 1000$) with hard segments based on PTMI. The sample codes and polymer structure were the same as discussed previously[31]. The compositions of samples used in this study are presented in *Table 1*. As in earlier reports[31], W_h is the hard segment concentration with one hard segment unit formally defined as part of the soft segment. W_h^* is the concentration of hard segments (the definition of this work), and m is the average hard segment length. The first number of the sample code corresponds to the weight percentage (nominal value) of hard segment. The final ratio corresponds to the ratio of terephthalate to isophthalate sequences in the hard segments. In this study, all of the hard segments contained exclusively isophthalate sequences, so the ratio of 0:100 is retained throughout.

D.s.c. was performed using a Perkin–Elmer DSC-7 calorimeter with model 7500 series computer station. The DSC-7 was run with liquid nitrogen cooling and helium purge (15 ml min^{-1}, 35 psi) of the sample chambers. Mercury (Aldrich Chemicals) and indium (Perkin–Elmer, rod stock) were used as calibrants for temperature and power. Baselines were determined using empty aluminium pans (TA Instruments) in both sample and reference chambers. In all cases the scan rate during heating was 20°C min^{-1}.

Samples for d.s.c. were formed from 6–12 mg discs cut from compression-moulded samples. Thermal lag was measured by the method of Richardson and Burrington[33] as a function of sample mass and temperature. Results were independent of copolymer composition, and corrections for non-linearity of temperature scale and absolute lag relative to the dynamic calibration were small, on the order of 0.1–0.6°C. In isothermal crystallization experiments, the sample was heated to the melt, held for 20 min, and then quenched to the crystallization temperature, T_c, for the indicated times. As discussed previously[31,34], changes in the intrinsic viscosity using the above-mentioned procedures were negligible. For crystallization times exceeding 3 h, the sample was rapidly transferred (< 1 min) to an air convection oven preheated to T_c, after quenching to T_c in the calorimeter. Temperature control of the oven was ±1°C. Samples were quenched after thermal treatment from T_c to temperatures about 100°C below T_g prior to the heating scan. Quenching rates were set to a nominal setting of 320°C min^{-1} although the actual quench rate was somewhat less than this. For samples treated in an oven, a brief transfer period (< 1 min) preceded the quench.

Glass transition calculations were performed graphically by a construction depicted previously[31]. Enthalpy changes on melting were calculated by integration of the area above the solid-to-melt baseline. This baseline was established by an iterative technique, which assumed that baseline recovery was governed by the fractional loss in crystallinity. No corrections for a temperature-dependent heat of fusion were applied[35]. Peak melting points were determined from the maximum in the baseline (solid–melt) subtracted endotherms.

Table 1 Description of samples

Sample	W_h	W_h^*	m
H30/0:100	0.29	0.433	3.1
H60/0:100	0.57	0.652	7.9
H80/0:100	0.8	0.838	22.2
H100/0:100	1	1	–

RESULTS

Homopolymer crystallization

Representative crystallization behaviour of the PTMI homopolymer, H100/0:100, is demonstrated by the d.s.c. scans taken after various lengths of time during isothermal crystallization at 106°C, as shown in *Figure 1*. These results illustrate that the d.s.c. experiments can follow the development of crystallinity in PTMI throughout the crystallization process, from the supercooled liquid to the completion of crystallization. The d.s.c. results show dual endotherms at all the crystallization temperatures investigated for PTMI. The higher temperature endotherm appears to develop at the earliest time, whereas the lower melting, 'annealing' endotherm appears to develop later.

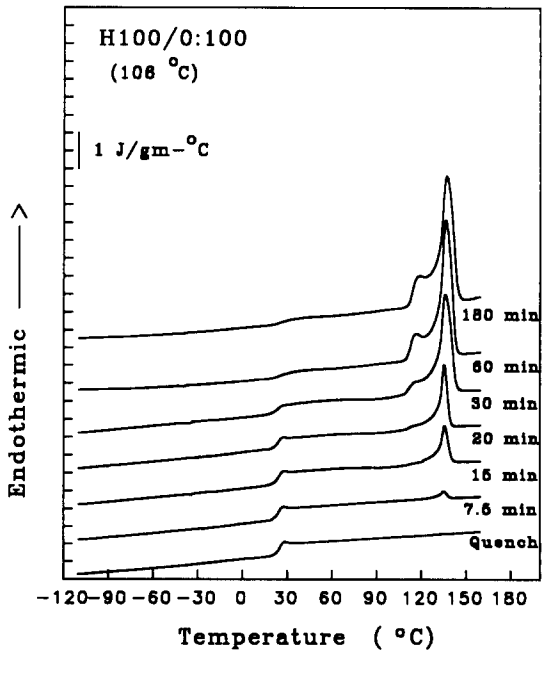

Figure 1 D.s.c. scan development of H100/0:100 during isothermal crystallization at 106°C

This behaviour is similar to that observed in other semi-crystalline polymers[35–38]. The 'annealing' endotherm appears before the completion of growth of the higher temperature endotherm. The relevant time-scales for crystallization are illustrated in *Figure 2* at high undercooling and *Figure 3* at low undercoolings. In these figures, the total area under both melting endotherms is shown as a function of the crystallization time. Crystallization occurs on the time-scale of approximately 30 min to several hours, with the maximum in crystallization rate observed between 66 and 86°C. For PTMI[31], the equilibrium melting point T_m° is 165 ± 5.4°C, suggesting that in terms of undercooling, the maximum crystallization rate occurs at $\Delta T \approx 90$°C.

The heat capacity change at T_g, ΔC_p ($J\,g^{-1}\,K^{-1}$), is normalized to the degree of crystallinity according to:

$$\Delta C_p^a = \Delta C_{p,obs}/(1 - X_c) \quad (1)$$

where ΔC_p^a is the calculated heat capacity change at T_g after normalization for the non-crystalline fraction, $\Delta C_{p,obs}$ is the experimentally observed heat capacity change at T_g when normalized to the total sample mass, and X_c is the d.s.c.-measured weight fraction crystallinity calculated according to:

$$X_c = \Delta H/\Delta H^\circ \quad (2)$$

The value of ΔH°, the enthalpy change on melting of the 100% crystalline material, is taken as $121.7\,J\,g^{-1}$. This value gives X_c results which match those given by wide angle X-ray scattering (WAXS)[31]. Values of ΔC_p^a for H100/0:100 are shown in *Figure 4* as a function of the crystallization temperature and the degree of crystallinity during crystallization (as measured by ΔH).

The experimental value for ΔC_p^a in the absence of crystallinity is $0.320 \pm 0.018\,J\,g^{-1}\,K^{-1}$, which is obtained after quenching from the melt[31]. *Figure 4* shows a slight over-prediction of the two-phase prediction suggested by equation (1). The results are independent of the crystallization temperature at low to moderate undercoolings,

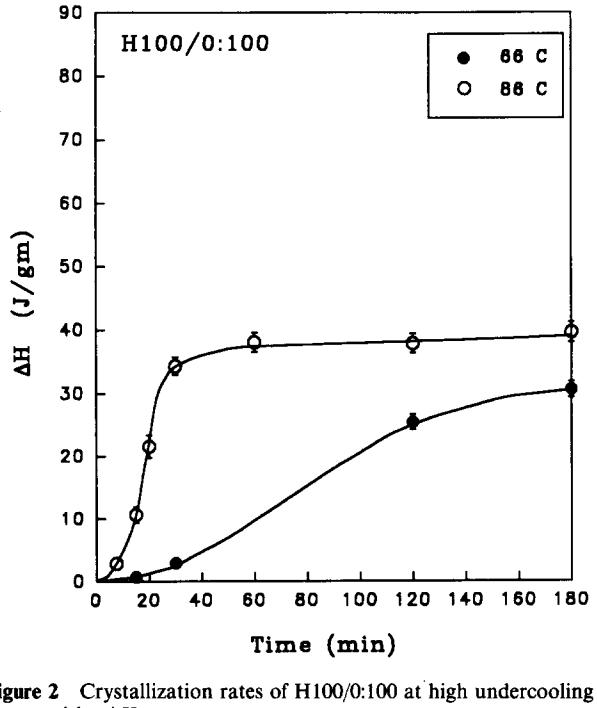

Figure 2 Crystallization rates of H100/0:100 at high undercooling as measured by ΔH

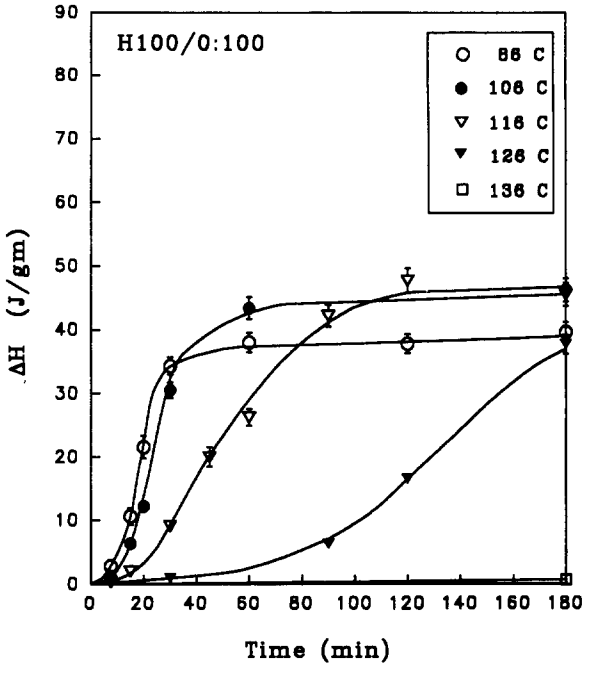

Figure 3 Crystallization rates of H100/0:100 at the indicated T_c as measured by ΔH

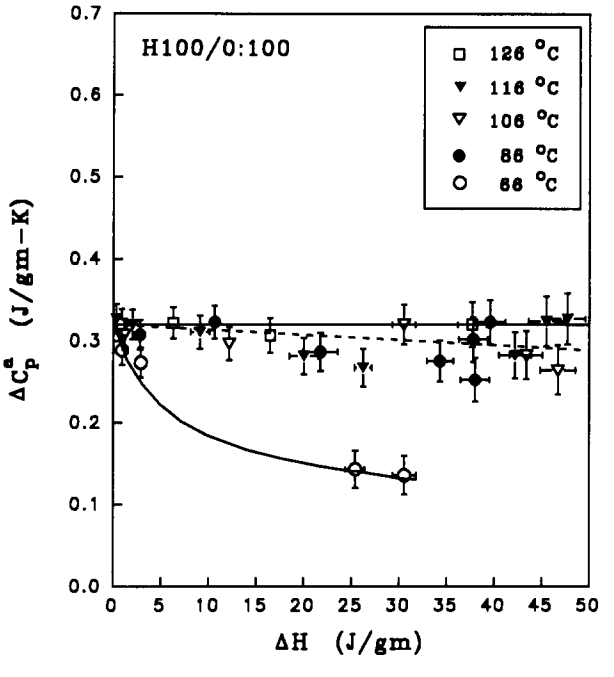

Figure 4 Correlation of the heat capacity change at T_g normalized by the amorphous content, ΔC_p^a, with the measured enthalpy change of melting, ΔH, during crystallization of H100/0:100

while a severe over-prediction of the two-phase model occurs on cooling below the temperature of maximum rate. This is seen in the data taken during crystallization at 66°C. The position of T_g as a function of the crystallization temperature and degree of crystallinity during crystallization is shown in *Figure 5*. An elevation in T_g occurs at the later stages of crystallization, and the degree of crystallinity required to cause this elevation decreases as the crystallization undercooling is increased.

Copolymer crystallization

Representative d.s.c. scans taken during crystallization are shown in *Figures 6–8* for H30/0:100, H60/0:100 and H80/0:100. The endotherm development seen during

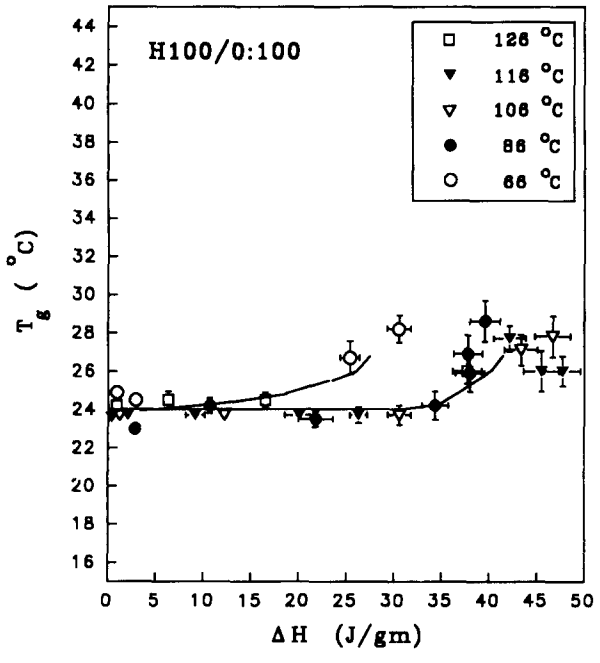

Figure 5 Correlation of T_g with the measured enthalpy change of melting, ΔH, during crystallization of H100/0:100

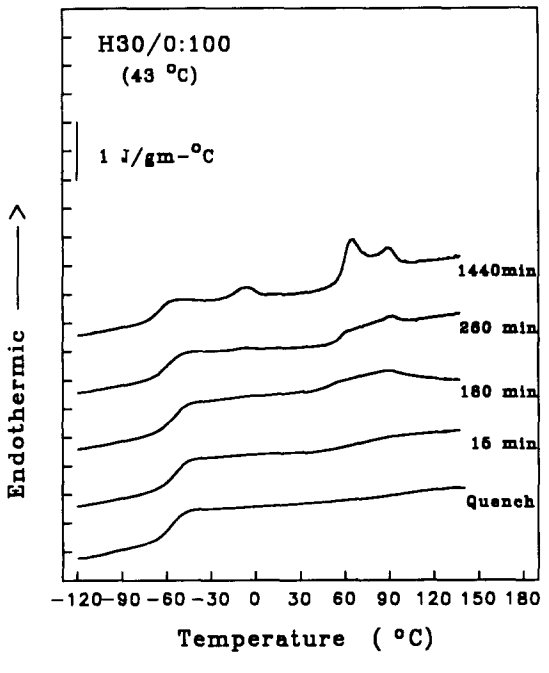

Figure 6 D.s.c. scan development of H30/0:100 during isothermal crystallization at 43°C

crystallization in the copolymers is quite similar to that of the homopolymer, suggesting that the multiple endotherm behaviour is a general characteristic of the hard segment. The details of the melting behaviour are sensitive to copolymer composition, however. The low temperature endotherm becomes increasingly pronounced as the hard segment concentration decreases. Similar observations have been made in poly(ether–ester) copolymers with mixed PTMI/PTMT hard segments as the concentration of the dominant crystallizing component in the hard segments was decreased[23,29,31]. Previous studies of the undercooling dependence on the melting behaviour have shown that at low undercoolings, the higher melting peak decreases with decreased hard segment concentration according to the Flory equation[31]. *Figure 9* shows, however, that the 'annealing' endotherm position is independent of copolymer composition irrespective of the temperature of crystallization.

Previous work[31] has shown that initially, after quenching from the melt, only a single composition-dependent T_g is observed, which can be described by mixed phase correlations for T_g and ΔC_p. The glass transition behaviour during crystallization in the copolymers presents some unique complications. As time is allowed for crystallization, hard segment sequences become incorporated into crystallites, which must alter the bulk composition of the amorphous regions. The

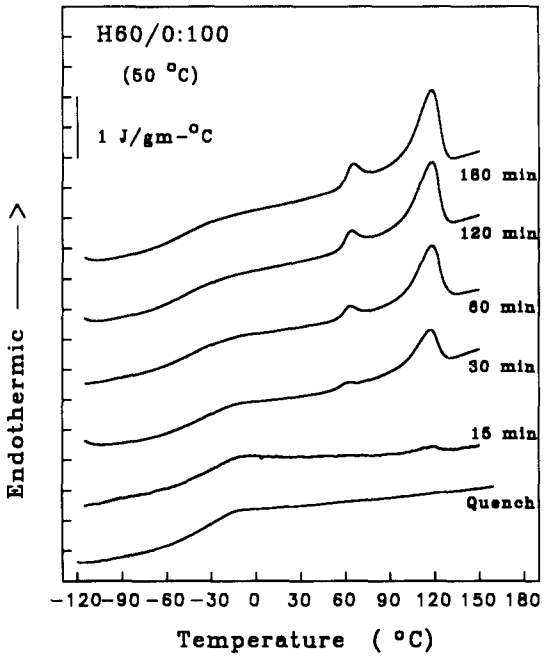

Figure 7 D.s.c. scan development of H60/0:100 during isothermal crystallization at 50°C

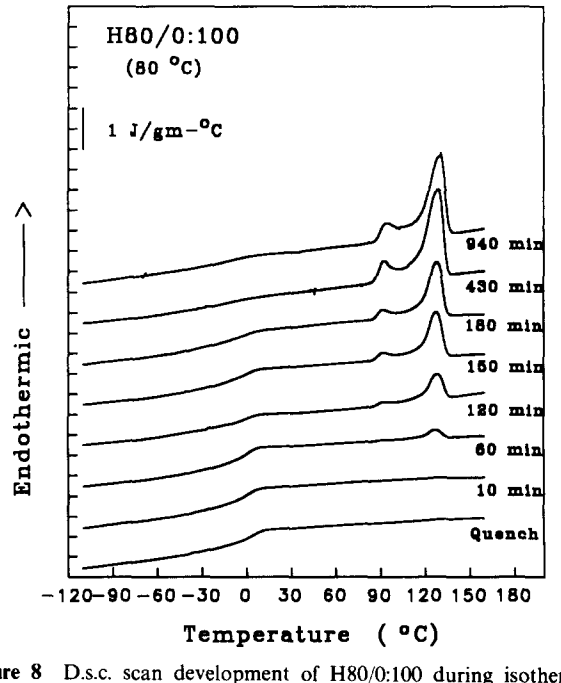

Figure 8 D.s.c. scan development of H80/0:100 during isothermal crystallization at 80°C

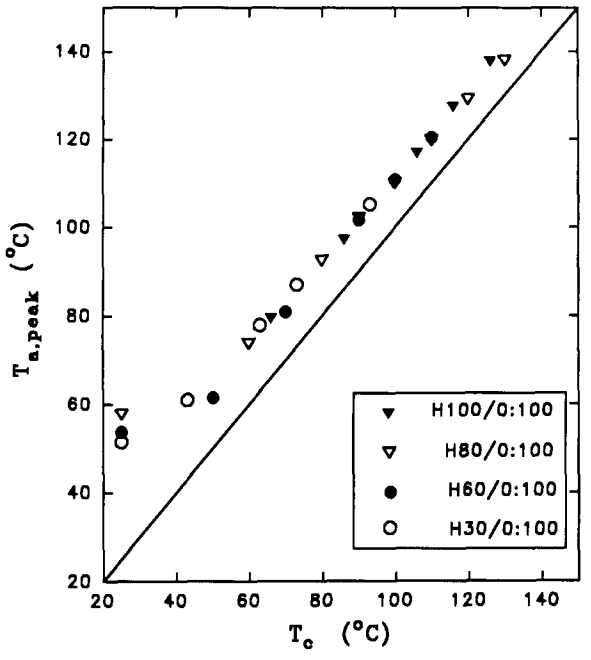

Figure 9 Dependence of annealing peak temperature on the crystallization temperature, T_c, for H30/0:100, H60/0:100, H80/0:100 and H100/0:100

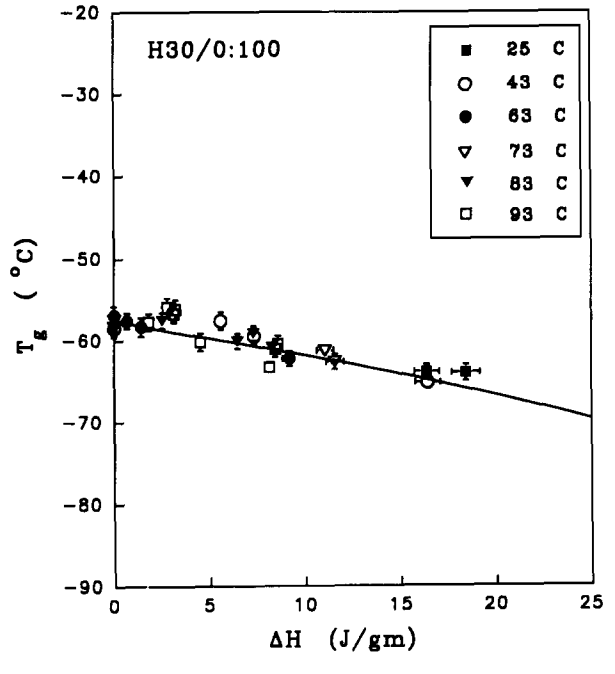

Figure 10 Correlation of T_g with the measured enthalpy change of melting, ΔH, during crystallization of H30/0:100. The solid line is derived from equations (3) and (4)

individual components may also demix if there is thermodynamic incompatibility of the dissimilar segment types. *Figures 10–12* show the T_g *versus* enthalpy change on melting, ΔH, as crystallization proceeds in H30/0:100, H60/0:100 and H80/0:100. The solid lines in *Figures 10–12* were calculated from the Gordon–Taylor equation[39,40]:

$$(1-W_h^a)(T_g-T_{g,s})+kW_h^a(T_g-T_{g,h})=0 \qquad (3)$$

where $T_{g,s}$ and $T_{g,h}$ are the glass transition temperatures of the soft and hard segments, respectively, and k is a constant. Previous work has determined these values to be −95.4°C, +24.0°C and 0.61, respectively, when equation (3) is applied to copolymers quenched from the melt[31]. The average hard segment concentration in the non-crystalline regions, W_h^a, can be estimated from the measured degree of crystallinity and the bulk hard segment concentration, W_h^*:

$$W_h^a=(W_h^*-X_c)/(1-X_c) \qquad (4)$$

Equations (3) and (4) assume a two-phase model composed of crystallites containing only PTMI sequences and non-crystalline regions composed of a mixture of the PTMO and PTMI sequences.

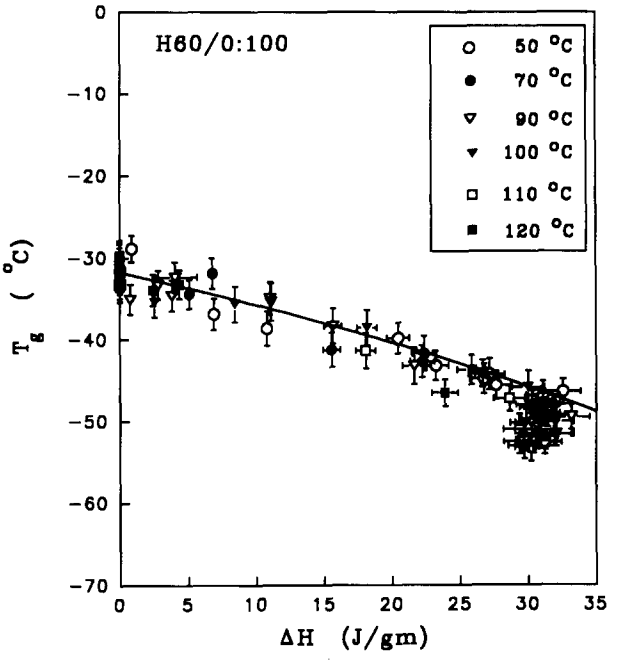

Figure 11 Correlation of T_g with the measured enthalpy change of melting, ΔH, during crystallization of H60/0:100. The solid line is derived from equations (3) and (4)

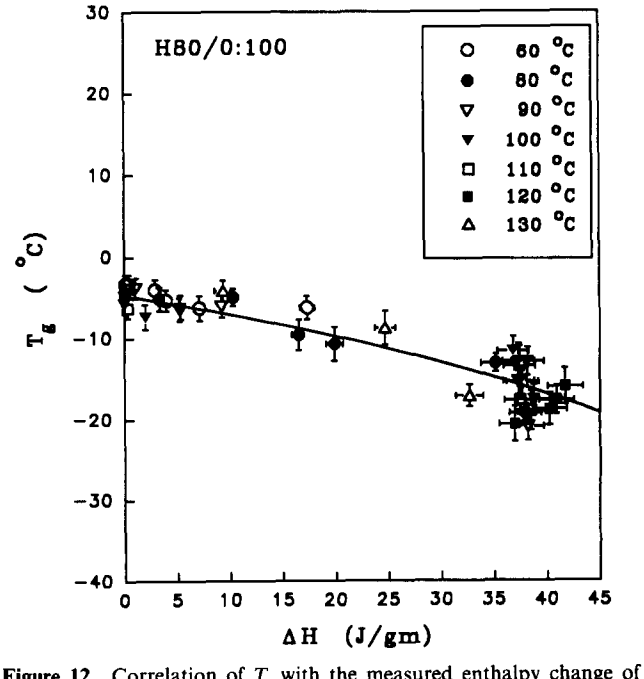

Figure 12 Correlation of T_g with the measured enthalpy change of melting, ΔH, during crystallization of H80/0:100. The solid line is derived from equations (3) and (4)

Figures 10–12 show that the T_g decreases during crystallization as hard segment units are removed from the amorphous regions and incorporated into the crystalline regions. This decrease is independent of the crystallization temperature for all of the copolymer compositions investigated, and indicates that the composition of the amorphous regions, and hence the T_g, is controlled primarily by crystallization of the hard segment sequences. This decrease is reasonably well described by equation (3) without fitting of the experimental data.

The ΔC_p^a data for the copolymers are shown in *Figures 13–15*. In the softer copolymers, as with the T_g data,

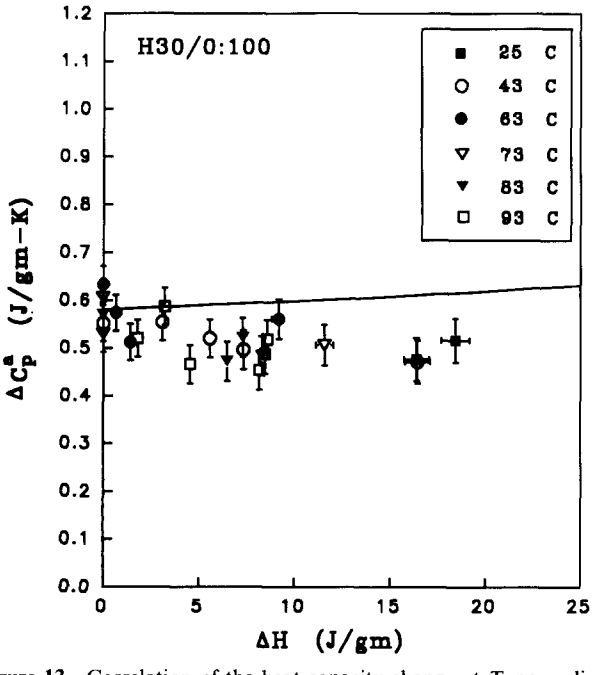

Figure 13 Correlation of the heat capacity change at T_g normalized by the amorphous content, ΔC_p^a, with the measured enthalpy change of melting, ΔH, during crystallization of H30/0:100. The solid line is derived from equations (4) and (5)

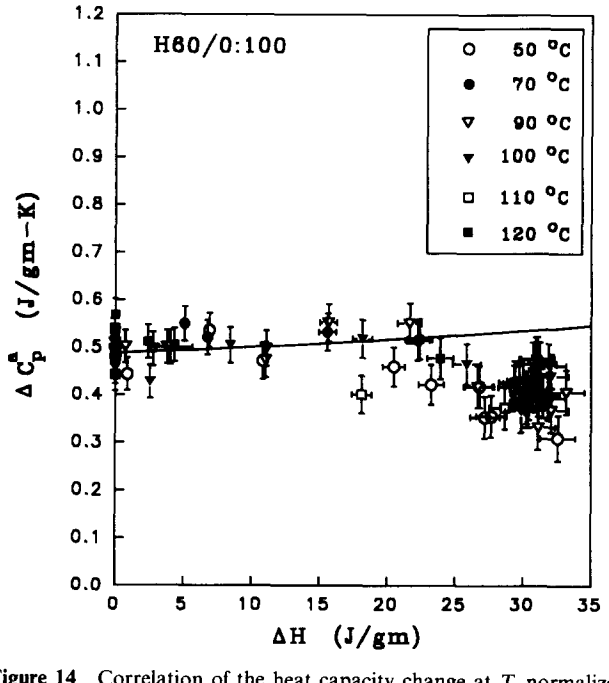

Figure 14 Correlation of the heat capacity change at T_g normalized by the amorphous content, ΔC_p^a, with the measured enthalpy change of melting, ΔH, during crystallization of H60/0:100. The solid line is derived from equations (4) and (5)

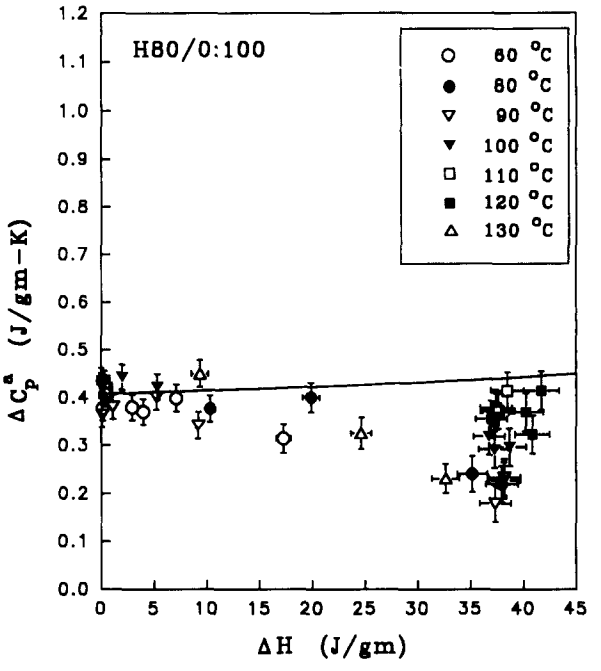

Figure 15 Correlation of the heat capacity change at T_g normalized by the amorphous content, ΔC_p^a, with the measured enthalpy change of melting, ΔH, during crystallization of H80/0:100. The solid line is derived from equations (4) and (5)

the ΔC_p^a results are independent of the crystallization temperature, being controlled principally by the degree of crystallinity. In H80/0:100, the temperature-independent behaviour observed in the softer copolymers appears to break down to some extent, as indicated by the wide spread of ΔC_p^a values at higher crystallinities. A similar effect, although somewhat sharper with respect to the crystallization temperature, is observed for the PTMI homopolymer in *Figure 4*. The solid line in *Figures 13–15* is the corresponding mixed-phase prediction for ΔC_p^a. This prediction was determined from:

$$\Delta C^a_{p,mix} = W_h^a \Delta C^o_{p,h} + (1 - W_h^a)\Delta C^o_{p,s} \quad (5)$$

where $\Delta C^o_{p,h}$ and $\Delta C^0_{p,s}$ are the pure component heat capacity change at T_g of the PTMI and PTMO sequences and are 0.320 ± 0.018 and $0.764 + 0.050\ J\ g^{-1}\ K^{-1}$, respectively[31]. After normalization for the non-crystalline content, equation (5) indicates that the heat capacity change should increase slightly with increasing degree of crystallinity owing to an enrichment of the PTMO concentration in the amorphous regions. For all of the copolymer compositions, the two-phase prediction with mixed amorphous regions, represented by equation (5), over-predicts the observed normalized heat capacity change at T_g. Similar behaviour was seen in *Figure 4* for the PTMI homopolymer, particularly at higher undercoolings.

DISCUSSION

The ΔC_p^a results shown in *Figure 4* indicate that the two-phase model applied to the PTMI homopolymer is an over-simplification. A possible explanation of the results is recognition of the role of crystalline regions as physical crosslinks, anchoring the non-crystalline chains at the crystalline lamellae. This might be expected to decrease the liquid heat capacity of the anchored chains leading to a reduced ΔC_p. Such an effect has been

noted by Ellis *et al.*[41] in a chemically crosslinked polystyrene system, showing decreased ΔC_p with increasing T_g and increased crosslink density. This effect appears sensitive to the nature of the crosslink as only modest changes in ΔC_p were observed in epoxies by Lee and McKenna[42] with large changes in T_g on crosslinking. This anchoring effect is clearly evident in *Figure 5* at the latter stages of crystallization. An increase of approximately 4°C in T_g is observed at higher crystallinity levels. The magnitude of this increase is independent of the crystallization temperature, but appears at reduced crystallinity levels for lower crystallization temperatures. Comparison of *Figure 4* and *Figure 5* shows that for the same increase in T_g, different values of ΔC_p^a are observed depending on the original crystallization temperature. This suggests that the discrepancy in ΔC_p^a is in general not correlated directly to the rise in T_g, and may be due to a mass balance discrepancy in the two-phase model.

Wunderlich and co-workers proposed the presence of immobile non-crystalline regions in a variety of semicrystalline systems[35,43,44]. The content of these regions was proposed to be related to the specific polymer type (chain flexibility) and the crystallization conditions. Generally, the discrepancy observed in ΔC_p^a is larger at higher undercooling, where the crystallite size is small and the surface area large[35]. Recent work by Huo and Cebe[45,46] suggests that in poly(phenylene sulfide) and PEEK, the rigid-amorphous fraction(s) partially gain mobility as the temperature is raised below the melting temperature. A similar notion of an extended range of mobilities in the amorphous regions of semicrystalline materials has been proposed by Struik[47,48] as an explanation of mechanical ageing response. Analogous interpretations can be suggested by the results presented in *Figure 4*. These results show that in H100/0:100 the discrepancy in ΔC_p^a appears to be closely related to the temperature of maximum crystallization rate, which lies between 66 and 86°C as indicated in *Figures 2* and *3*.

As with the homopolymer, similar discrepancies in the values of ΔC_p^a are observed in the copolymers during crystallization. The heat capacity change in the copolymers also contains the possible contribution of phase separation of the dissimilar, yet non-crystalline, segment types. This contribution to the heat capacity change has been used as a measure of the extent of phase separation in multiblock copolymers[10,49,50]. Without assumption as to the origin of the discrepancy in the copolymers, the amorphous regions can be crudely defined in terms of a non-crystalline fraction $(1-X_c)$, which is the sum of a mobile fraction, W_m, and an immobile fraction, W_i, at the experimentally observed low temperature T_g. This assignment assumes crystalline regions pure in the polyester component, and the presence of a fraction W_i. This fraction may have a variety of morphological origins such as partial phase separation, interfacial content or constrained chains. If the concentration of hard segments in the fraction W_i is taken as f_i, then the concentration of hard segments in the mobile fraction at $T_g(f_m)$ is given in equation (6). The predicted normalized heat capacity change at $T_g(\Delta C_{p,m}^a)$ is given by equation (7):

$$f_m = \frac{(W_h^* - X_c - f_i W_i)}{(1 - X_c - W_i)} \tag{6}$$

$$\Delta C_{p,m}^a = \Delta C_{p,s}^o + f_m(\Delta C_{p,h}^o - \Delta C_{p,s}^o) \tag{7}$$

The relationship between the observed normalized heat capacity change (ΔC_p^a) in *Figures 13–15*, and that for the generalized 'mobile' fraction represented by equation (7) is given by:

$$\Delta C_p^a \frac{(1-X_c)}{(1-X_c-W_i)} = \Delta C_{p,m}^a \tag{8}$$

The difference, $\Delta C_{p,h}^o - \Delta C_{p,s}^o$, is the slope of the experimentally obtained correlation of ΔC_p *versus* W_h^* derived from the melt-quenched copolymers, while $\Delta C_{p,s}^o$ is the intercept. This slope and intercept can be derived from previously published data as $-0.424\,J\,g^{-1}\,K^{-1}$ and $0.764\,J\,g^{-1}\,K^{-1}$, respectively[31].

Inserting equations (6) and (7) into equation (8) gives the following result:

$$\Delta C_p^a = \left[\Delta C_{p,s}^o + \frac{(W_h^* - X_c)}{(1-X_c)}(\Delta C_{p,h}^o - \Delta C_{p,s}^o)\right] - \left[\frac{W_i}{(1-X_c)}(\Delta C_{p,s}^o + f_i(\Delta C_{p,h}^o - \Delta C_{p,s}^o))\right] \tag{9}$$

The meaning of equation (9) is that the observed normalized heat capacity increment is the phase-mixed contribution predicted from degree of crystallinity estimates (equation (5)), less the contribution of material that does not participate in the main relaxation associated with the glass transition. Equation (9) is general, with no inherent assumptions about the origin of the 'immobile' material at T_g other than the assumption that the soft segment is excluded from the crystalline regions. In poly(ether–ester) copolymers with PTMT hard segments, the crystalline regions are generally considered to be relatively pure in the polyester segment owing to the close agreement of WAXS patterns with the homopolymer pattern over a wide range of copolymer compositions[14,15,21–23]. Equation (9) can be further rearranged as:

$$\frac{W_i}{(1-X_c)} = \frac{\Delta C_{p,mix}^a - \Delta C_p^a}{\Delta C_{p,s}^o + f_i(\Delta C_{p,h}^o - \Delta C_{p,s}^o)} \tag{10}$$

where $\Delta C_{p,mix}^a$ is the first term in equation (9). The morphological origins of the discrepancy in the heat capacity change at T_g in the copolymers cannot be unambiguously determined by d.s.c. data alone. Equation (10) describes the heat capacity results in terms of two unknown parameters, W_i and f_i, assuming that the effect is due solely to a mass balance discrepancy. On physical grounds, f_i should be bounded by the mixed-amorphous phase limit and the pure PTMI limit, as described by:

$$\frac{W_h^* - X_c}{1 - X_c} < f_i < 1 \tag{11}$$

Table 2 lists values of W_i calculated from equation (10) for the limiting values of f_i given in equation (11); both the mixed phase limit and the demixed limit are included. To perform this estimate, an average value of ΔC_p^a was taken at the late stages of crystallization. For H80/0:100, this corresponds to data taken near the middle of the experimental crystallization temperature range. Also shown in *Table 2* are the predicted and observed values of T_g for the mobile regions. *Table 2* suggests that the limit $f_i = 1$ is inconsistent with the T_g data. This suggests that the concentration of hard segments in the 'immobile' regions approximates much more closely to the mixed-phase predictions, and indicates that the observed

Table 2 Limiting calculations of W_i

Sample	W_i (mixed limit)	W_i (demixed limit)	T_g predicted (°C) (mixed limit)	T_g predicted (°C) (demixed limit)	T_g observed (°C)
H100/0:100	0.06	–	–	–	–
H80/0:100	0.21	0.27	−16.1	−36.7	−16.5
H60/0:100	0.18	0.28	−46	−74.2	−49
H30/0:100	0.21	0.33	−66.9	−95.4	−64.4

discrepancy is probably not due to thermodynamic-driven phase separation in the amorphous regions. This conclusion is also supported by the value of T_g during crystallization in the copolymers.

Figures 10–12 indicate that the T_g is independent of the crystallization temperature for all copolymer compositions. As an example[34], H60/0:100 crystallizes over a period of about 3 h at 50°C and 24 h at 120°C. If demixing were to occur prior to crystallization of the hard segment sequences, a temperature-independent T_g would not be expected unless crystallization was effectively instantaneous after demixing. Under isothermal conditions, the slow crystallization behaviour of the isophthalate hard segments and homopolymer appears inconsistent with this scenario. This indicates that the T_g, and hence the composition of the amorphous regions, is controlled by crystallization of the hard segments. Less convincing, but supportive, is the calculation of the two-phase model shown in *Figures 10–12*. Considering the approximations in the assumed mixing rule (equation (3), and the uncertainties in determining absolute crystallinities, the predictions of the T_g during crystallization are reasonable without fitting of the data. A slight negative deviation is seen in the data of H60/0:100 in *Figure 11* and *Table 2*, although again the T_g values are independent of the crystallization temperature.

The temperature-independent T_g and reasonable predictions of the T_g during crystallization suggest highly phase-mixed amorphous regions during crystallization. It has been established from the earliest studies of poly(ether–ester) copolymers that the T_g of fully crystallized copolymers with PTMT hard segments decreases continuously with a decrease in the bulk hard segment concentration[14,17]. The results have been adequately correlated by a Gordon–Taylor equation format[17]. Owing to the rapid crystallization of the PTMT sequences, the T_g cannot be monitored unambiguously during crystallization. These experiments establish the 'path dependence' of the T_g in this class of materials with PTMI hard segments. Earlier melt scattering studies of PTMI/PTMO copolymers also suggested a single-phase melt that persisted to temperatures below the hard segment melting point[31]. Although not unambiguous, these results suggest that the observed heat capacity change in the copolymers is of a similar origin to that found in the homopolymer. This conclusion requires that a certain fraction of the non-crystalline material does not participate in the relaxation associated with the main glass transition and, as discussed earlier, is of a similar composition to the amorphous fraction which does relax. In H60/0:100, the largest compositional disparity is observed (see *Table 2*), but this disparity appears far removed from the limit of 'demixed' phases. The softer copolymers have reduced T_g (increased mobility at T_c), larger long spacings and amorphous layer thickness values[34], and decreased crystallinity. In the softest copolymers, an observation of a discrepancy in ΔC_p^a, suggests that the material which is 'immobile' at T_g is not due to free chains, but rather may be due to chains immobilized by the crystallization process, such as interfacial and/or tie molecules. This is also consistent with the apparent 'mixed-phase' limit of this fraction, in contrast to that observed in some semicrystalline blend systems[51–53]. In addition to the strong compatibility of the short-segment sequences in these copolymers[31], the chemical connectivity of the constituent blocks along the chain requires that the soft segment 'diluent' be connected to the crystal surface. Accordingly, it is not unreasonable to assume that the probability that a chain exiting from the crystal surface is a hard segment will be of the same order of magnitude as the concentration of hard segments in the amorphous regions.

The ΔC_p^a results can equivalently be interpreted as due to partial phase separation. If the quantity W_i is assigned to the 'hard phase', then in the limit of $f_i = W_h^a$, the mass fraction and hard segment concentration of the 'soft phase', M_s and $\phi_s = W_h^a$, and the mass fraction and hard segment concentration of the 'hard phase', M_h and ϕ_h, can be calculated from the following equations:

$$M_s = 1 - X_c - W_i \tag{12}$$

$$\phi_s = W_h^a \tag{13}$$

$$M_h = X_c + W_i \tag{14}$$

$$\phi_h = \frac{(X_c + W_i f_i)}{(X_c + W_i)} \tag{15}$$

The evolution of the 'soft phase' and 'hard phase' structure during morphology development can be estimated using the Gordon–Taylor equation prediction (*Figure 11*), and the evaluation of $W_i = fn(X_c)$ from *Figure 14*. The results are shown schematically in *Figure 16*. Using these definitions, M_s decreases while M_h increases during the course of crystallization (given by a lever rule in *Figure 16*), while both ϕ_h and ϕ_s are observed to decrease during crystallization. This is not an intuitive situation based on thermodynamic-driven separation of the 'phases', but is rather the result of a crystallization-driven phase separation. As discussed earlier, this interpretation is supported by the observation that the glass transition temperatures in the copolymers are independent of the crystallization temperature, being controlled by the degree of crystallization.

While the distinction between 'phase separated' or 'immobile' is largely one of language, the current data suggest that the observed deviation from the two-phase description is of physical origin associated with the non-equilibrium mobilities created through the crystallization process, rather than of thermodynamic origin. *Figure 17* shows the calculation of W_i (a lower bound) in

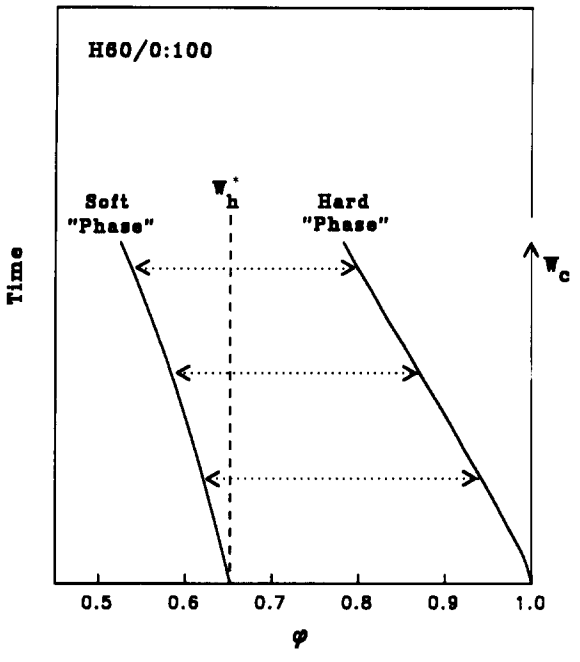

Figure 16 Schematic of the evolution of 'soft phase' and 'hard phase' structure during crystallization of H60/0:100, from equations (12)–(15). ϕ is the hard segment weight fraction in the respective 'phases' (ϕ_h or ϕ_s); the mass fractions M_s, M_h are calculated from a lever rule during crystallization. The 'hard phase' contains the hard segment crystallites ($\phi = 1$) and the fraction W_i (equation (10)) in the mixed phase limit (equation (11))

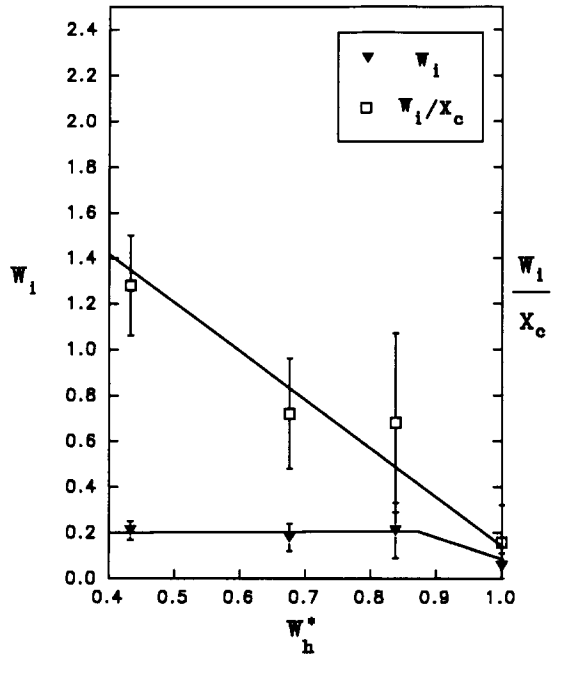

Figure 17 Estimation of W_i and W_i/X_c for H30/0:100, H60/0:100, H80/0:100 and H100/0:100 at the completion of crystallization

the mixed-phase limit (equation (11)) both on an absolute basis and normalized to the degree of crystallinity. Less chain folding and a more diffuse crystal core are expected in the copolymers, leading to higher values of W_i for a given crystallinity level. On a normalized basis, the increase of W_i/X_c with decreasing hard segment content appears to have an analogue in studies of polyethylene copolymers, where the 'interfacial' content was observed to increase markedly[54,55] and surface fold energy increased[56] with increasing co-unit content. Increased heterogeneity in PTMT/PTMO copolymers was noted in SAXS studies by Perago *et al.*[57]. Recent interpretations by Apostolov and Fakirov[58] have also suggested that the fraction of tie molecules increases as the hard segment concentration decreases. In this sense, the reduction in hard segment concentration appears to have a similar effect on the crystal core/surface morphology as crystallization of the PTMI homopolymer at high undercooling, where the corresponding values for W_i and W_i/X_c are 0.43 ± 0.05 and 1.71 ± 0.21, respectively. These conclusions are applied at the glass transition temperature of the copolymers under investigation. The morphological state discussed above for temperatures at the glass transition temperatures may be related to the numerous observations from dynamic mechanical experiments which show varying breadth of the loss tangent and loss modulus at T_g with changing composition[17,19], although this work cannot directly address the temperature dependence of the calculated W_i.

As seen in *Figure 1* and *Figures 6–8*, dual endotherms are displayed in both the PTMI homopolymer and PTMI/PTMO copolymers. This indicates that this feature of the melting behaviour is a characteristic of the hard segment, and that a uniquely 'copolymeric' explanation of multiple endotherm behaviour is not necessary in the PTMI/PTMO copolymers. Previous variable heating rate experiments of the PTMI homopolymer have shown that, although a reorganization mechanism may be a contributing factor to the dual endotherm behaviour, the asymmetry of the melting region is characteristic of the morphology[31]. *Figure 9* indicates that the crystallization temperature determines the lower crystallite stability limit, and hence the breadth of the melting range. This is reflected in the extreme sensitivity of the annealing endotherm position to the crystallization temperature, and the independence of the annealing endotherm position on composition at a fixed crystallization temperature (*Figure 9*). One possible explanation of the annealing endotherm is a model assuming a secondary crystallization process similar to other proposals in the literature[38,59,60]. According to a secondary crystallization model[34], the contrasting time dependencies of the two endotherms could be rationalized in terms of separate growth processes. Although the dual endotherms are predominantly a characteristic of the hard segment, there are subtleties in the behaviour which are sensitive to copolymer composition. In the context of a secondary crystallization model of the dual endotherm behaviour, the increased predominance of the annealing endotherm with decreasing hard segment concentration may reflect a reduced relative rate of the primary growth/nucleation process due to the presence of the polyether, and the increased mobility in the partially solidified regions of the copolymers.

CONCLUSIONS

The slow rate of crystallization of poly(tetramethylene isophthalate) (PTMI), and multiblock copolymers with poly(tetramethylene oxide) (PTMI/PTMO), enables the phase separation/crystallization process to be monitored by d.s.c. from the supercooled liquid to the completion of crystallization over a wide range of crystallization temperatures. A model is suggested whereby phase separation in the copolymers proceeds in a manner

similar to crystallization of the homopolymer. The glass transition data during crystallization suggest a phase state in the copolymers consistent with a two-phase model composed of PTMI crystallites and phase-mixed amorphous regions with respect to composition, although the amorphous regions are inhomogeneous, containing regions possessing non-equilibrium mobilities. This latter aspect of the morphology is sensitive to copolymer composition and is related to the influence of the soft segment on the crystal core/surface morphology in a manner similar to the homopolymer crystallized at high undercooling. Although subtleties in the melting endotherms are sensitive to copolymer composition, the experimentally observed multiple endotherm behaviour in the PTMI homopolymer and the PTMI/PTMO copolymers is a characteristic of the hard segment.

ACKNOWLEDGEMENTS

The authors thank Dr J. Michael McKenna (Polymer Automotive, E.I. duPont de Nemours & Co.) for synthesis of the polymers used in this work. Partial funding was provided by the NSF Division of Materials Research (DMR-90-16959).

REFERENCES

1 Gibson, P. E., Vallance, M. A. and Cooper, S. L. in 'Developments in Block Copolymers' (Ed. I. Goodman), Applied Science Series, Elsevier, London, 1982
2 Adams, R. K. and Hoeschele, G. K. in 'Thermoplastic Elastomers' (Eds N. R. Legge, G. Holden and H. E. Schroeder), Hanser Publishers, New York, 1987
3 Wilkes, G. L. and Wildnaur, R. *J. Appl. Phys.* 1975, **46**, 4148
4 Kwei, T. K. *J. Appl. Polym. Sci.* 1982, **27**, 2891
5 Galambos, A. F. PhD Thesis, Princeton University, 1989
6 Li, Y., Gao, T. and Chu, B. *Macromolecules* 1992, **25**, 1737
7 Seymour, R. W. and Cooper, S. L. *Macromolecules* 1973, **6**, 48
8 Hesketh, T. R., Van Bogart, Van J. W. C. and Cooper, S. L. *Polym. Eng. Sci.* 1980, **20**, 190
9 Van Bogart, Van J. W. C., Bleumke, D. A. and Cooper, S. L. *Polymer* 1981, 22, 1428
10 Leung, L. M. and Koberstein, J. T. *Macromolecules* 1986, **19**, 706
11 Koberstein, J. T. and Russell, T. P. *Macromolecules* 1986, **19**, 714
12 Koberstein, J. T. and Galambos, A. F. *Macromolecules* 1992, **25**, 5618
13 Van Bogart, J. W. C., Gibson, P. E. and Cooper, S. L. *J. Polym. Sci., Polym. Phys. Edn* 1983, **21**, 65
14 Cella, R. J. *J. Polym. Sci. C* 1973, **42**, 727
15 Buck, W. H., Cella, R. J., Gladding, E. K. and Wolfe, J. R. Jr *J. Polym. Sci. C* 1974, **48**, 47
16 Seymour, R. W., Overton, J. R. and Corley, L. S. *Macromolecules* 1975, **8**, 331
17 Lilaonitkul, A. and Cooper, S. L. *Rubber Chem. Technol.* 1977, **50**, 1
18 Zhu, L. and Wegner, G. *Makromol. Chem.* 1981, **182**, 3625
19 Zhu, L., Wegner, G. and Bandara, U. *Makromol. Chem.* 1981, **182**, 3639
20 Bandara, U. and Drosher, M. *Colloid Polym. Sci.* 1983, **261**, 26
21 Vallance, M. A. and Cooper, S. L. *Macromolecules* 1984, **17**, 1208
22 Briber, R. M. and Thomas, E. L. *Polymer* 1985, **26**, 8
23 Castles, J. L., Vallance, M. A., McKenna, J. M. and Cooper, S. L. *J. Polym. Sci., Polym. Phys. Edn* 1985, **23**, 2119
24 Fakirov, S. and Gogeva, T. *Makromol. Chem.* 1990, **191**, 603
25 Stockton, W. B. MS Thesis, Princeton University, 1988
26 Stevenson, J. C. and Cooper, S. L. *J. Polym. Sci., Polym. Phys. Edn* 1988, **26**, 953
27 Stein, R. S. and Misra, A. *J. Polym. Sci., Polym. Phys. Edn* 1980, **18**, 327
28 Yeh, J. T. and Runt, J. *J. Polym. Sci., Polym. Phys. Edn* 1989, **27**, 1543
29 Stevenson, J. C. PhD Thesis, University of Wisconsin-Madison, 1987
30 Stevenson, J. C. and Cooper, S. L. *Macromolecules* 1988, **21**, 1309
31 Phillips, R. A., McKenna, J. M. and Cooper, S. L. *J. Polym. Sci., Polym. Phys. Edn* 1994, **32**, 791
32 Witsiepe, W. K. *Adv. Chem. Ser.* 1973, **129**, 39
33 Richardson, M. J. and Burrington, P. *J. Therm. Anal.* 1974, **6**, 345
34 Phillips, R. A. PhD Thesis, University of Wisconsin-Madison, 1992
35 Wunderlich, B. 'Thermal Analysis', Academic Press, Boston, 1990
36 Cheng, S. Z. D., Cao, M. Y. and Wunderlich, B. *Macromolecules* 1986, **19**, 1868
37 Gardner, K. C. H., Hsiao, B. S., Matheson, R. R. Jr and Wood, B. A. *Polymer* 1992, **33**, 2483
38 Chung, J. S. and Cebe, P. *Polymer* 1992, **33**, 2312
39 Gordon, M. S. and Taylor, J. S. *J. Appl. Chem.* 1952, **2**, 493
40 Wood, L. A. *J. Polym. Sci.* 1958, **28**, 319
41 Ellis, T. S., Karasz, F. E. and ten Brinke, G. J. *J. Appl. Polym. Sci.* 1983, **28**, 23
42 Lee, A. and McKenna, G. B. *Polymer* 1988, **29**, 1812
43 Suzuki, H., Grebowicz, J. and Wunderlich, B. *Makromol. Chem.* 1985, **186**, 1109
44 Cheng, S. Z. D., Wu, Z. Q. and Wunderlich, B. *Macromolecules* 1987, **20**, 2802
45 Huo, P. and Cebe, P. *J. Polym. Sci., Polym. Phys. Edn* 1992, **30**, 239
46 Huo, P. and Cebe, P. *Macromolecules* 1992, **25**, 902
47 Struik, L. C. E. *Polymer* 1987, **28**, 1521
48 Struik, L. C. E. *Polymer* 1987, **28**, 1534
49 Camberlin, Y. and Pascault, J. P. *J. Polym. Sci., Polym. Phys. Edn* 1984, **22**, 1835
50 Wagener, K. B., Matayabas, J. C. Jr and Wanigatunga, S. *Macromolecules* 1989, **22**, 3211
51 Hahn, B. R., Hermann-Shonherr, O. and Wendorff, J. J. *Polymer* 1987, **28**, 201
52 Russell, T. P., Ito, H. and Wignall, G. D. *Macromolecules* 1988, **21**, 1703
53 Kumar, S. K. and Yoon, D. Y. *Macromolecules* 1991, **24**, 5414
54 Mandelkern, L. *Polym. J.* 1985, **17**, 337
55 Alamo, R. G., Viers, B. D. and Mandelkern, L. *Macromolecules* 1993, **26**, 5470
56 Darras, O. and Seguela, R. *Polymer* 1993, **34**, 2946
57 Pergao, G., Cesari, M. and Vitali, R. *J. Appl. Polym. Sci.* 1984, **29**, 1157
58 Apostolov, A. A. and Fakirov, S. *J. Macromol. Sci.-Phys.* 1992, **B31**, 329
59 Bassett, D. C., Olley, R. H. and Raheil, I. A. M. *Polymer* 1988, **29**, 1945
60 Hsiao, B. S. Gardner, K. C. H., Wu, D. Q. and Chu, B. *Polymer* 1993, **34**, 3986